New Journal of Physics
The open access journal at the forefront of physics

Deutsche Physikalische Gesellschaft **DPG**

IOP Institute of Physics

Published in partnership with: Deutsche Physikalische Gesellschaft and the Institute of Physics

PAPER

Photon BEC with thermo-optic interaction at dimensional crossover

Enrico Stein[*] [ID] and Axel Pelster [ID]

Department of Physics and Research Center OPTIMAS, Technische Universität Kaiserslautern, Erwin-Schrödinger-Straße 46, 67663 Kaiserslautern, Germany

[*] Author to whom any correspondence should be addressed.

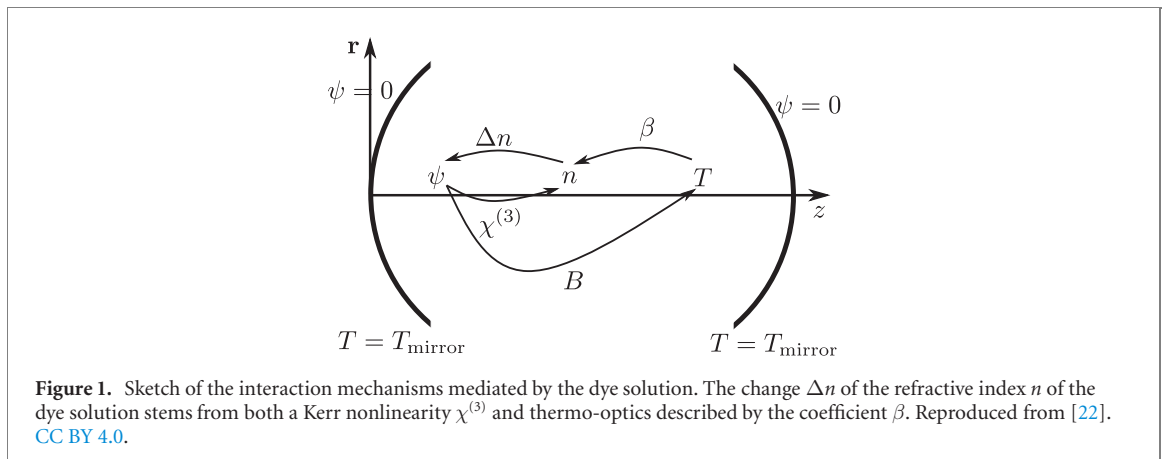E-mail: estein@rhrk.uni-kl.de and axel.pelster@physik.uni-kl.de

Abstract

Since the advent of experiments with photon Bose–Einstein condensates (phBECs) in dye-filled microcavities in 2010, many investigations have focussed upon the emerging effective photon–photon interaction. Despite its smallness, it can be identified to stem from two physically distinct mechanisms. On the one hand, a Kerr nonlinearity of the dye medium yields a photon–photon contact interaction. On the other hand, a heating of the dye medium leads to an additional thermo-optic interaction, which is both delayed and non-local. The latter turns out to represent the leading contribution to the effective interaction for the current 2D experiments. Here we analyse theoretically how the effective photon–photon interaction increases when the system dimension is reduced from 2D to 1D. To this end, we consider an anisotropic harmonic trapping potential and determine via a variational approach how the properties of the phBEC in general, and both aforementioned interaction mechanisms in particular, change with increasing anisotropy. We find that the thermo-optic interaction strength increases at first linearly with the trap aspect ratio and later on saturates at a certain value of the trap aspect ratio. Furthermore, in the strong 1D limit the roles of both interactions get reversed as the thermo-optic interaction remains saturated and the contact Kerr interaction becomes the leading interaction mechanism. Finally, we discuss how the predicted effects can be measured experimentally.

1. Introduction

Ultracold atomic quantum systems in dimensions lower than three bear interesting physics [1, 2]. In 2D an interacting Bose gas can undergo a crossover from a Bose–Einstein condensate to a Berezinskii–Kosterlitz–Thouless phase [3–5], where vortex and anti-vortex pairs are produced and can move through the gas. In one-dimensional systems large phase fluctuations are detected [6], which induce an algebraic decay of the correlation function, in contrast to an exponential decay in higher dimensions. Moreover, it is also known that the effective interaction strength increases by reducing the dimension of the system [7]. For systems of bosonic atoms the dimensional crossover has already been investigated broadly from 3D to 2D [8] and even down to 1D [9, 10]. The question of the effective system dimension can be reduced to a discussion of the relevant length scales [11]. Provided that the healing length of a three-dimensional condensate confined by an axially symmetrical trap is larger than the axial width, the system is effectively two-dimensional. In case that the in-plane radius is smaller than the healing length, the system is quasi-1D.

For photon Bose–Einstein condensates (phBEC) [12], however, such a dimensional crossover has so far not been realised. As these kinds of experiments are conducted in a microcavity, they turn out to be already two-dimensional. It is expected that the crossover to 1D can be achieved experimentally by writing an anisotropic harmonic confining potential directly on the mirror [13–15]. This should yield a simple control of the trap anisotropy, which then allows to freeze out the higher dimension as has already been shown in

Figure 1. Sketch of the interaction mechanisms mediated by the dye solution. The change Δn of the refractive index n of the dye solution stems from both a Kerr nonlinearity $\chi^{(3)}$ and thermo-optics described by the coefficient β. Reproduced from [22]. CC BY 4.0.

the theoretical study [16]. Thus, such photonic systems constitute a useful platform to investigate the crossover from higher to lower dimensions.

Following this line of reasoning necessitates a glimpse into whether a true Bose–Einstein condensate in the one-dimensional harmonic trap exists at all. Although in an early work [17] it was shown via a semiclassical ansatz, that an ideal gas cannot Bose–Einstein condense in such a trap, a full quantum mechanical investigation has, indeed, shown the existence of such a condensate [18]. In the later work [19] these two former results have been brought together by generalising the semiclassical ansatz from [17], see also [16] for a detailed discussion. However, in this paper we focus on the $T = 0$ situation for a weakly interacting Bose gas. In the realm of quantum degenerate Bose gases in 1D it has been pointed out in [20], that for $T = 0$ one always deals with a true Bose–Einstein condensate. Therefore, we will always use the term BEC throughout this paper.

In the corresponding experimental set-up, photons are trapped in a dye-filled cavity and, due to the contact with the dye, the photon gas is allowed to thermalise [21] and finally to Bose–Einstein condense [12]. Moreover, the dye solution leads also to an effective photon–photon interaction via two mechanisms, as is depicted in figure 1. One is the Kerr effect, which is due to a nonlinearity $\chi^{(3)}$ of the solvent molecules, where a change of the refractive index $\Delta n \propto |\psi|^2$ leads to an effective contact interaction. The second mechanism for the effective photon–photon interaction is the thermo-optic effect. Since the quantum efficiency of the dye lies below one, some electronic excitations of the dye molecules are converted into phononic excitations due to the electron–phonon coupling in the molecule. Since these are also distributed through the solvent, this leads to a net heating of the dye solution. This changes the refractive index of the dye solution according to the thermo-optic coefficient β and, thus, contributes to the effective photon–photon interaction.

It turns out that the thermo-optic interaction is the leading contribution in the current 2D experiments, whereas the Kerr interaction is completely negligible in this situation. However, the total interaction strength is still quite small as the dimensionless interaction strength amounts to about $\tilde{g} = mg/\hbar^2 \sim 10^{-4}$ [12, 23]. Therefore, effects of stronger interaction like superfluidity are not yet observable and even the thermodynamics turns out to be not affected by the interaction [24]. This finding motivated our previous study [16], where we investigated as a first step the dimensional crossover of a non-interacting photon BEC from 2D to 1D by determining its thermodynamic properties and by extracting from them the effective system dimension for a given temperature and trap aspect ratio. In a second step, it is now crucial to search for mechanisms to increase the effective photon–photon interaction. In this respect we already found in the former theoretical study [22] the intriguing result that the strength of the thermo-optic interaction increases quadratically with the lateral extension of the cavity mirrors. However, as this would be quite laborious to achieve experimentally, we explore here an alternative mechanism, which relies on increasing the effective photon–photon interaction strength by reducing the system dimension from 2D to 1D. As it is already known that this increases effectively the contact interaction [25], our main focus lies hereby on the question how the dimensional crossover modifies the thermo-optic interaction.

To this end, we start by introducing in section 2 a coupled system of mean-field equations describing the steady state of both the phBEC ground state and the temperature, which is produced by the phBEC and which conversely affects the photon–photon interaction. Instead of straight-forwardly solving this coupled system of equations by numerical means, we construct an approximate solution within a semi-analytic procedure as follows. At first, we eliminate the temperature degrees of freedom by using the corresponding Green's function and determine with this the resulting energy functional for the condensate. As the profile

of the photon condensate wave function is a Gaussian in the non-interacting case, it is reasonable to assume that this profile remains to be valid also in the mutual presence of both Kerr and thermo-optic interaction. Therefore, within a variational approach, we minimise the condensate energy function with respect to the widths of the used Gaussian trial function in section 3. Solving the corresponding self-consistency conditions for these widths, it turns out that the dimensional crossover can physically be divided into three different regimes. The first one corresponds to small trap aspect ratios λ and shows, as expected, an increase of the thermo-optic interaction strength. In the second regime for intermediate λ, the thermo-optic interaction turns out to saturate, as here the condensate width in the squeezed direction is smaller than the characteristic length scale of the temperature diffusion. Finally, in the third regime for large λ the contact Kerr interaction turns out to take over the leading role in the effective photon–photon interaction. At the end, we discuss that the respective strengths of Kerr and thermo-optic interaction can not only be extracted from the condensate widths but also from analysing the energy in the quasi 1D regime. To conclude this work, we also apply this method in section 4 to the crossover in a potential, where in addition to the tightening of the confinement in a single direction the potential in the second direction is loosened. This potential bears the advantage of a constant particle density in the trap centre, since by only tightening a single direction the photon density in the trap centre steadily increases, which yields in the experimental situation to mirror loss processes and, consequently, to multimode condensates. Here we find, that both the thermo-optic and the Kerr interaction increase linearly with the trap-aspect ration, such that a much larger effective photon–photon interaction strength might be achieved. With this we demonstrate how the dimensional crossover depends on the details of the chosen potential.

2. General equations

Our starting point for describing the photon BEC ground state is the mean-field theory worked out in reference [22], see figure 1. There we used a set of two coupled equations in order to describe both the photon BEC wave function in the microcavity and the heat diffusion in the dye solution inducing the thermo optics. However, for the current purpose, we consider two modifications of this mean-field theory. On the one hand, we neglect the imaginary part of the equation for the condensate wave function, as this simply determines the photon number N. On the other hand, we also need to take the Kerr effect into account, which gives rise to an additional contact interaction term in the equation for the photon BEC wave function. In total, the steady state of the condensate is, thus, described by

$$\mu\psi = \left(-\frac{\hbar^2\nabla^2}{2m} + V + g_K|\psi|^2 + \gamma\Delta T\right)\psi, \tag{1}$$

where m represents the effective photon mass and V describes the external potential. The strength of the Kerr interaction is given by g_K and the energy shift due to the temperature difference ΔT between the actual intracavity temperature and the room temperature is intermediated by the parameter γ, which is proportional to the thermo-optic coefficient β from figure 1 [22]. Furthermore, the photon BEC wave function is normalised according to $\int \mathrm{d}^2x|\psi|^2 = N$.

The steady state of the temperature difference ΔT, which is produced by the photon condensate due to non-perfect absorption–reemission cycles and which diffuses through the cavity, is described by the diffusion equation

$$\Delta T = \tau\mathcal{D}\nabla^2\Delta T + \sigma\tau B|\psi|^2. \tag{2}$$

Here τ denotes the longitudinal relaxation time stemming from the diffusion along the optical axis, see reference [22] and the appendix therein, $\mathcal{D}$ stands for the diffusion coefficient of the temperature, and the heating of the dye solution is modelled via the heating rate B. Furthermore, the duty cycle σ describes that the experiment operates with a pulsed pump laser, whereas our theoretical description works with a continuous pump for reaching the steady state. This modification is needed here, as the temperature necessitates several experimental cycles to achieve its steady state [22].

2.1. Elimination of temperature difference
As a first step, we eliminate the temperature difference as a degree of freedom from our description. To this end, we formally solve the diffusion equation (2) according to

$$\Delta T(\mathbf{x}) = \sigma\tau B \int \mathrm{d}^2x' \, \mathcal{G}(\mathbf{x}-\mathbf{x}')|\psi(\mathbf{x}')|^2, \tag{3}$$

where we have introduced the Green's function $\mathcal{G}(\mathbf{x})$. Its Fourier transform $\tilde{\mathcal{G}}(\mathbf{k})$ reads

$$\tilde{\mathcal{G}}(\mathbf{k}) = \frac{1}{\tau \mathcal{D} \mathbf{k}^2 + 1}, \tag{4}$$

so we conclude for the real space

$$\mathcal{G}(\mathbf{x}) = \int \frac{\mathrm{d}^2 k}{4\pi^2} \frac{e^{\mathrm{i}\mathbf{k}\cdot\mathbf{x}}}{\tau \mathcal{D} \mathbf{k}^2 + 1}. \tag{5}$$

In order to evaluate the integral we use the Schwinger parametrisation [26]

$$\int_0^\infty \mathrm{d}t \, e^{-at} = \frac{1}{a}, \tag{6}$$

and have then

$$\mathcal{G}(\mathbf{x}) = \int_0^\infty \mathrm{d}t \int \frac{\mathrm{d}^2 k}{4\pi^2} e^{-(1+\tau \mathcal{D} \mathbf{k}^2)t + \mathrm{i}\mathbf{k}\cdot\mathbf{x}}. \tag{7}$$

As the integral over $\mathbf{k}$ represents now a Gaussian, we can calculate it and find

$$\mathcal{G}(\mathbf{x}) = \int_0^\infty \mathrm{d}t \, \mathcal{G}(\mathbf{x}, t), \tag{8}$$

with the integrand

$$\mathcal{G}(\mathbf{x}, t) = \frac{e^{-\mathbf{x}^2/(4l_{\mathrm{diff}}^2 t) - t}}{4\pi l_{\mathrm{diff}}^2 t}. \tag{9}$$

Here $l_{\mathrm{diff}} = \sqrt{\tau \mathcal{D}}$ represents the diffusion length and the Schwinger parameter t corresponds physically to the time in units of the longitudinal relaxation time τ. We recognise expression (9) to be the Green's function of the time-dependent diffusion equation. Whereas at initial time the Green's function (9) reduces to the delta function, i.e.

$$\mathcal{G}(\mathbf{x}, 0) = \delta(\mathbf{x}), \tag{10}$$

summing (9) over all times finally yields the steady-state Green's function (8). Evaluating the remaining Schwinger integral in equation (8) leads to a modified Bessel function of the second kind K_0 [27, (3.471.9)]:

$$\mathcal{G}(\mathbf{x}) = \frac{\|\mathbf{x}\|}{4\pi l_{\mathrm{diff}}^2} K_0 \left(\sqrt{\frac{\|\mathbf{x}\|}{l_{\mathrm{diff}}}} \right). \tag{11}$$

Whereas the initial Green's function (10) has its maximum at the origin $\mathbf{x} = \mathbf{0}$, the steady-state Green's function (11) is maximal at a circle, whose radius is given by $\|\mathbf{x}\| \sim l_{\mathrm{diff}}$. Although we have an explicit expression (11) for the Green's function (8), the Schwinger integral representation (9) turns out to be more advantageous for the following analytic calculation, such that we prefer to use it instead throughout the remainder of this paper. Taking this into account, equation (3) can be written as

$$\Delta T(\mathbf{x}) = \sigma \tau B \int_0^\infty \mathrm{d}t \int \mathrm{d}^2 x' \, \mathcal{G}(\mathbf{x} - \mathbf{x}', t) |\psi(\mathbf{x}')|^2. \tag{12}$$

With this the steady-state profile of the temperature difference is given due to diffusion by the photon density.

2.2. Photon functional

Using the formal solution of the diffusion equation (2) in the form (12), the photon BEC wave function equation (1) goes over into

$$\mu\psi = \left[-\frac{\hbar^2 \nabla^2}{2m} + V + g_{\mathrm{K}} |\psi|^2 + g_{\mathrm{T}} \int_0^\infty \mathrm{d}t \int \mathrm{d}^2 x' \, \mathcal{G}(\mathbf{x} - \mathbf{x}', t) |\psi(\mathbf{x}')|^2 \right] \psi. \tag{13}$$

Here the resulting thermo-optic interaction strength is defined as [22]

$$g_{\mathrm{T}} = \sigma \gamma \tau B, \tag{14}$$

and is, thus, determined by various material properties of the dye solution. As a next step, we determine the energy functional corresponding to equation (13), which turns out to consist of three parts:

$$E[\psi^*, \psi] = E_0[\psi^*, \psi] + E_{\mathrm{K}}[\psi^*, \psi] + E_{\mathrm{T}}[\psi^*, \psi]. \tag{15}$$

The first one describes both the kinetic and the potential energy of the photon BEC and reads

$$E_0[\psi^*, \psi] = \int d^2x \left[\frac{\hbar^2}{2m} |\nabla \psi|^2 + V|\psi|^2 \right], \tag{16}$$

whereas the second one,

$$E_K[\psi^*, \psi] = \frac{g_K}{2} \int d^2x |\psi|^4, \tag{17}$$

represents the contact Kerr interaction. The last term comprises the thermo-optic effects via

$$E_T[\psi^*, \psi] = \frac{g_T}{2} \int_0^\infty dt \int d^2x \int d^2x' \, \mathcal{G}(\mathbf{x} - \mathbf{x}', t)|\psi(\mathbf{x}')|^2|\psi(\mathbf{x})|^2. \tag{18}$$

In the following we aim at minimising the energy functional (15) for a harmonic confinement along the dimensional crossover within a variational approach, similar to our preceding work [22].

3. Variational approach

We express the harmonic potential in the form

$$V = \frac{m\Omega^2}{2}(x^2 + \lambda^4 y^2), \tag{19}$$

where the trap aspect ratio $\lambda = l_x/l_y$ determines the ratio of the oscillator length $l_i = \sqrt{\hbar/(m\Omega_i)}$ with $i = x, y$ in the respective dimensions and $\Omega = \Omega_x$ is the trapping frequency in x-direction. As the photon condensate wave function is a Gaussian in the non-interacting case, it is reasonable to assume that this profile remains to be valid also in the mutual presence of both Kerr and thermo-optic interaction. Therefore, the variational ansatz for the phBEC ground-state wave function reads

$$\psi = \sqrt{\frac{\lambda N}{\alpha_x \alpha_y \pi l_x^2}} \, \exp\left[-\frac{1}{2l_x^2} \left(\frac{x^2}{\alpha_x^2} + \lambda^2 \frac{y^2}{\alpha_y^2} \right) \right], \tag{20}$$

where we treat α_x, α_y as the corresponding variational parameters. Note that due to this choice, these parameters are dimensionless and $\alpha_x = \alpha_y = 1$ describes the non-interacting case. Inserting the ansatz (20) into the functional (15) yields the energy as a function of the two variational parameters and the ratio $\lambda_{\text{diff}} = l_x/l_{\text{diff}}$ of the oscillator length l_x and the diffusion length l_{diff}:

$$E(\alpha_x, \alpha_y) = N\hbar\Omega \left[\frac{1}{4}\left(\frac{1}{\alpha_x^2} + \frac{\lambda^2}{\alpha_y^2} \right) + \frac{1}{4}\left(\alpha_x^2 + \lambda^2\alpha_y^2 \right) + \frac{\tilde{g}_K \lambda N}{4\pi\alpha_x\alpha_y} \right.$$

$$\left. + \frac{\tilde{g}_T \lambda N}{4\pi\alpha_x\alpha_y} \int_0^\infty dt \, \frac{e^{-t}}{\sqrt{[1 + 2t/(\lambda_{\text{diff}}^2\alpha_x^2)][1 + 2t\lambda^2/(\lambda_{\text{diff}}^2\alpha_y^2)]}} \right]. \tag{21}$$

Note that we have defined here the dimensionless interaction strength $\tilde{g}_\bullet = mg_\bullet/\hbar^2$. Thus, by performing the derivative of the function (21) either with respect to α_x or with respect to α_y we can calculate the corresponding equations for the variational parameters and obtain
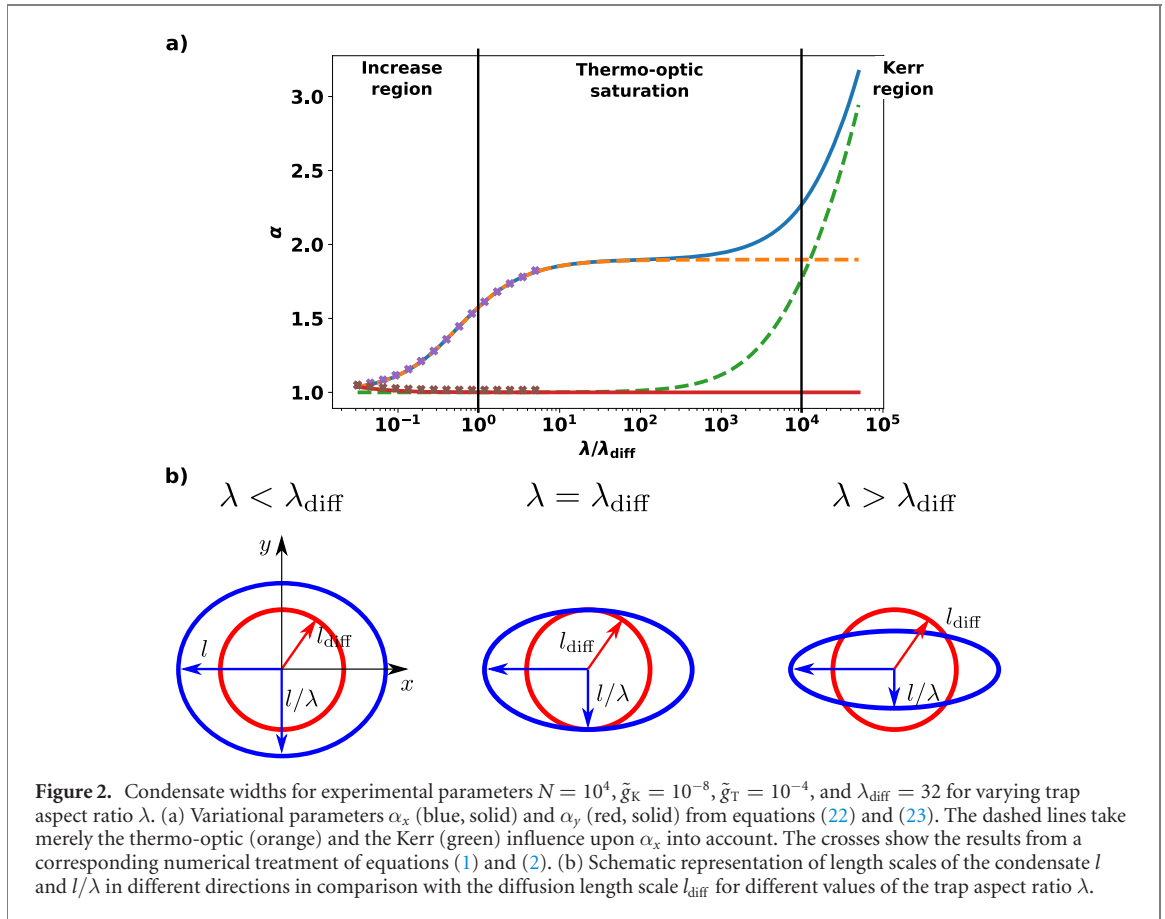
$$\alpha_x = \frac{1}{\alpha_x^3} + \frac{\tilde{g}_K \lambda N}{2\pi\alpha_x^2\alpha_y} + \frac{\tilde{g}_T \lambda N}{2\pi\alpha_x^2\alpha_y} \int_0^\infty dt \, \frac{e^{-t}}{\sqrt{[1 + 2t/(\lambda_{\text{diff}}^2\alpha_x^2)]^3[1 + 2t\lambda^2/(\lambda_{\text{diff}}^2\alpha_y^2)]}}, \tag{22}$$

for the x direction and in the squeezed y direction we have

$$\lambda^2\alpha_y = \frac{\lambda^2}{\alpha_y^3} + \frac{\tilde{g}_K \lambda N}{2\pi\alpha_x\alpha_y^2} + \frac{\tilde{g}_T \lambda N}{2\pi\alpha_x\alpha_y^2} \int_0^\infty dt \, \frac{e^{-t}}{\sqrt{[1 + 2t/(\lambda_{\text{diff}}^2\alpha_x^2)][1 + 2t\lambda^2/(\lambda_{\text{diff}}^2\alpha_y^2)]^3}}. \tag{23}$$

3.1. General solution

At first, we discuss the general solution of the self-consistency equations (22) and (23) as depicted in figure 2(a). We see that, as the trap aspect ratio λ increases, the variational parameter α_y approaches the value 1. This indicates that in this direction the broadening due to the interaction gets negligible, which

Figure 2. Condensate widths for experimental parameters $N = 10^4$, $\tilde{g}_K = 10^{-8}$, $\tilde{g}_T = 10^{-4}$, and $\lambda_{\text{diff}} = 32$ for varying trap aspect ratio λ. (a) Variational parameters α_x (blue, solid) and α_y (red, solid) from equations (22) and (23). The dashed lines take merely the thermo-optic (orange) and the Kerr (green) influence upon α_x into account. The crosses show the results from a corresponding numerical treatment of equations (1) and (2). (b) Schematic representation of length scales of the condensate l and l/λ in different directions in comparison with the diffusion length scale l_{diff} for different values of the trap aspect ratio λ.

means that the system behaves effectively one-dimensional. On the other hand, we observe a much more complex behaviour for the variational parameter α_x, where we discern in total three regions. For small trap aspect ratios λ the parameter α_x starts to grow, which is a characteristic sign of increasing interaction. Then, for intermediate $\lambda \sim \lambda_{\text{diff}}$, we find that the variational parameter α_x saturates, which signals a saturation of the interaction. And finally, for large trap aspect ratio λ, the variational parameter α_x increases again. We can understand this behaviour in more detail by separating the different interaction mechanisms numerically. The green and the red dashed line show the width by only taking the thermo-optic interaction and the Kerr interaction into account, respectively. We note, that, indeed, the thermo-optic interaction is the dominant interaction effect for small λ and saturates at $\lambda \sim \lambda_{\text{diff}}$. The Kerr interaction, on the other hand, behaves differently. Its contribution for small trap aspect ratio λ is negligible, but becomes stronger than the thermo-optic interaction at $\lambda \gtrsim \lambda_{\text{Kerr}} = \lambda_{\text{diff}} g_T / g_K$. This threefold behaviour is schematically shown in figure 2(b) by depicting the length scales of the condensate l and l/λ in different directions in comparison with the diffusion length scale l_{diff} for different values of the trap aspect ratio λ. Note that the particular role of the diffusion length scale l_{diff} can be traced back to the steady-state Green function (11), which is maximal at the circle with radius proportional to l_{diff}.

In order to support these findings, a numerical evaluation of equations (1) and (2) has been performed. Our numerics is based on an imaginary time split-step Fourier method, where the propagation with respect to the Laplacian appearing in (1) is done in the Fourier space and the remaining propagation takes place in the real space. Furthermore, the actual temperature distribution defined via the convolution integral (3) is also calculated in Fourier space using the Green's function (4). The used space–time discretisation is chosen such that for a given trap aspect ratio λ the phBEC wavefunction can also be resolved in the squeezed direction. Thus, after a sufficiently long propagation in imaginary time we can calculate the widths $q_x = \sqrt{2\langle x^2 \rangle}$ and $q_y = \sqrt{2\langle y^2 \rangle}$ from the resulting steady-state photon distribution. From the variational ansatz (20) we see, that the variational parameter α_x can directly be identified with the width q_x, whereas for the y direction we have $\alpha_y = \lambda q_y$. As we see in figure 2 our numerical results agree well with the results obtained from the variational equations (22) and (23). However, due to the increasing numerical effort, we have only compare the results for trap aspect ratios up to $\lambda = 5\lambda_{\text{diff}}$. In the following we discuss our findings in more detail from an analytical point of view.

3.2. Isotropic case

In the isotropic case we have $\lambda = 1$ and $\alpha_x = \alpha_y = :\alpha$, so equations (22) and (23) reduce to the single equation

$$\alpha = \frac{1}{\alpha^3} + \frac{\tilde{g}_K N}{2\pi\alpha^3} + \frac{\tilde{g}_T N}{2\pi\alpha^3} \int_0^\infty \mathrm{d}t \, \frac{e^{-t}}{(1 + 2t/\lambda_{\text{diff}}^2\alpha^2)^2}. \tag{24}$$

For the parameters of the Bonn experiment [12, 23] we estimate that $\lambda_{\text{diff}}^2 \sim 10^3 \gg 1$. Furthermore, the exponential in the integral leads to an effective cutoff of the integral for $t \sim 1$. Then the term $2t/\lambda_{\text{diff}}^2\alpha^2$ in the denominator can be neglected, since it only contributes to the integral at times $t \sim \alpha^2\lambda_{\text{diff}}^2/2 \gg 1$. With this we can calculate approximately the integral and conclude that α is determined by the algebraic equation

$$\alpha \approx \frac{1}{\alpha^3} + \frac{\tilde{g}_K N}{2\pi\alpha^3} + \frac{\tilde{g}_T N}{2\pi\alpha^3}. \tag{25}$$

Here the thermo-optic interaction behaves exactly as the Kerr interaction, as the influence of the diffusion dropped out. Furthermore, we can solve equation (25) for the variational parameter and obtain

$$\alpha = \sqrt[4]{1 + \frac{(\tilde{g}_K + \tilde{g}_T)N}{2\pi}}, \tag{26}$$

which we already obtained in the former work [22].

3.3. Quasi 1D case

Now we deal with the opposite situation, where the system is quasi-one-dimensional and determine at first for which trap aspect ratios λ this regime starts. To this end we read off from figure 2(a) that already for $\lambda \ll \lambda_{\text{diff}}$ we have $\alpha_y \approx 1$, which is a sign that in the squeezed direction the influence of the interaction is negligible. In this case the sum of kinetic and potential energy $E_y \approx N\hbar\Omega\lambda^2/2$ stored in the squeezed spatial degree of freedom is proportional to the square of the trap aspect ratio, whereas the interaction energy $E_{\text{int}} = E_K + E_T$ increases linearly with λ according to expression (21). Indeed, in this regime the contribution of the Kerr interaction can be neglected in comparison to the thermo-optic interaction according to figure 2(a). For the remaining integral we can apply the same approximation as in section 3.2, resulting finally in $E_{\text{int}} \approx \hbar\Omega\tilde{g}_T\lambda N/(4\pi\alpha_x)$. A further inspection of figure 2 reveals that we can roughly approximate $\alpha_x \approx 1$ in this regime as well. Thus, as the quasi-1D region amounts to the inequality $E_y \gg E_{\text{int}}$, we obtain the criterion

$$\lambda \gg \lambda_{\text{1D}} = \frac{\tilde{g}_T N}{2\pi}. \tag{27}$$

As current photon BEC experiments are characterized by $\tilde{g}_T = 10^{-4}$ and a maximal photon number $N = 10^5$, the 1D criterion (27) is basically fulfiled slightly above the 2D case $\lambda = 1$.

We proceed now to larger values of the trap aspect ratio λ, where we can still assume $\alpha_y \approx 1$, according to figure 2(a). We can now determine α_x self-consistently from equation (22), yielding

$$\alpha_x \approx \frac{1}{\alpha_x^3} + \frac{\tilde{g}_K \lambda N}{2\pi\alpha_x^2} + \frac{\tilde{g}_T \lambda N}{2\pi\alpha_x^2} \int_0^\infty \mathrm{d}t \, \frac{e^{-t}}{\sqrt{(1 + 2t/\lambda_{\text{diff}}^2\alpha_x^2)^3(1 + 2t\lambda^2/\lambda_{\text{diff}}^2)}}. \tag{28}$$
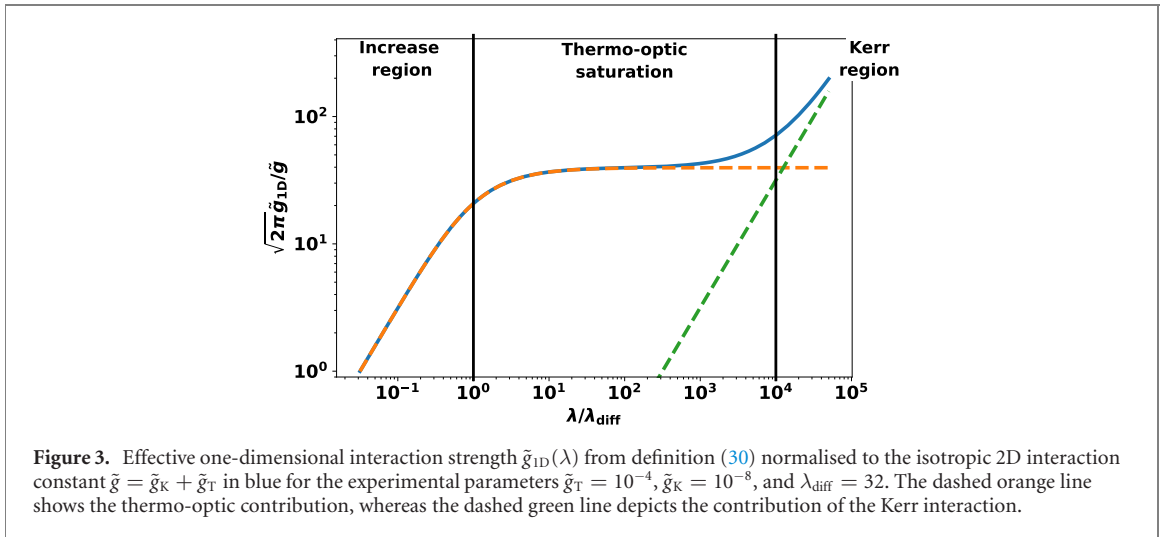
This integral is simplified along similar lines as in section 3.2, and it reduces to

$$\alpha_x^4 \approx 1 + \frac{\tilde{g}_{\text{1D}}(\lambda)N}{\sqrt{2\pi}}\alpha_x, \tag{29}$$

where we have introduced the effective 1D interaction strength inspired by a comparison with equation (A.4):

$$\tilde{g}_{\text{1D}}(\lambda) = \frac{1}{\sqrt{2\pi}}\left[\tilde{g}_K\lambda + \tilde{g}_T\lambda_{\text{diff}}\sqrt{\frac{\pi}{2}}e^{\lambda_{\text{diff}}^2/(2\lambda^2)}\mathrm{erfc}\left(\frac{\lambda_{\text{diff}}}{\sqrt{2}\lambda}\right)\right]. \tag{30}$$

We note that the contribution of the thermo-optic interaction is determined by the ratio $\lambda/\lambda_{\text{diff}} = \lambda l_{\text{diff}}/l_x$, i.e. the ratio of the diffusion length l_{diff} and the oscillator length in the squeezed y direction l_x/λ. Figure 3 depicts the total effective 1D interaction strength $\tilde{g}_{\text{1D}}(\lambda)$ from equation (30) as a function of λ. Also here we note the aforementioned three different regions of the crossover. For small trap aspect ratio λ the thermo-optic interaction, which gives here the leading contribution, increases and then indeed, as stated above, saturates. But for $\lambda > \lambda_{\text{Kerr}} = \lambda_{\text{diff}}\tilde{g}_T/\tilde{g}_K$ the Kerr interaction takes over and the total interaction grows again.

Figure 3. Effective one-dimensional interaction strength $\tilde{g}_{1D}(\lambda)$ from definition (30) normalised to the isotropic 2D interaction constant $\tilde{g} = \tilde{g}_K + \tilde{g}_T$ in blue for the experimental parameters $\tilde{g}_T = 10^{-4}$, $\tilde{g}_K = 10^{-8}$, and $\lambda_{diff} = 32$. The dashed orange line shows the thermo-optic contribution, whereas the dashed green line depicts the contribution of the Kerr interaction.

Let us now discuss these findings in more detail. For small trap aspect ratio, i.e. $\lambda \ll \lambda_{diff}$, we can approximate equation (30) by

$$\tilde{g}_{1D,0}(\lambda) \approx \frac{1}{\sqrt{2\pi}} \left(\tilde{g}_K + \tilde{g}_T \right) \lambda, \tag{31}$$

and in this case the thermo-optic interaction behaves like the Kerr interaction showing a linear increase in λ. The reason for this is that here the diffusion length is negligible compared to the condensate width in both x and y direction. Thus, the heat produced by the condensate only diffuses within a region where the condensate wave function does not vary, such that the thermo-optic interaction behaves approximately as a local contact interaction. On the other hand, once we have entered deeply the quasi-1D regime, i.e. $\lambda \gg \lambda_{diff}$, the effective 1D interaction strength (30) is given by

$$\tilde{g}_{1D,\infty}(\lambda) \approx \frac{1}{\sqrt{2\pi}} \left(\tilde{g}_K \lambda + \tilde{g}_{T,\infty} \right). \tag{32}$$

Thus, in this limit the thermo-optic part of the interaction strength no longer depends on the trap aspect ratio λ and saturates at the value

$$\tilde{g}_{T,\infty} = \tilde{g}_T \lambda_{diff}, \tag{33}$$

which is fixed by the geometry of the experiment and by the used solvent. This is due to the fact that here the width of the condensate in the squeezed direction l_x/λ is much smaller than the diffusion length l_{diff} and, thus, the heat being produced by the condensate diffuses through the dye medium to regions where no condensate exists, cf figure 2. This heat, therefore, cannot contribute to the interaction, such that the thermo-optic interaction saturates. For the Kerr contribution, however, the situation does not change and the total interaction strength still shows according to equation (32) a linear dependency in the trap aspect ratio λ.

Note that it is currently reasonably to expect achieving experimentally a trap anisotropy of at most $\lambda \sim 10^2 \lambda_{diff}$ [28]. From figure 1 we read off that in this case the Kerr interaction is still negligible and that the total effective 1D interaction is due to the thermo-optic effect. Thus, the maximally achievable effective 1D interaction strength $\tilde{g}_{1D,\infty}^{exp}$ reads, with the help of expressions (32) and (33)
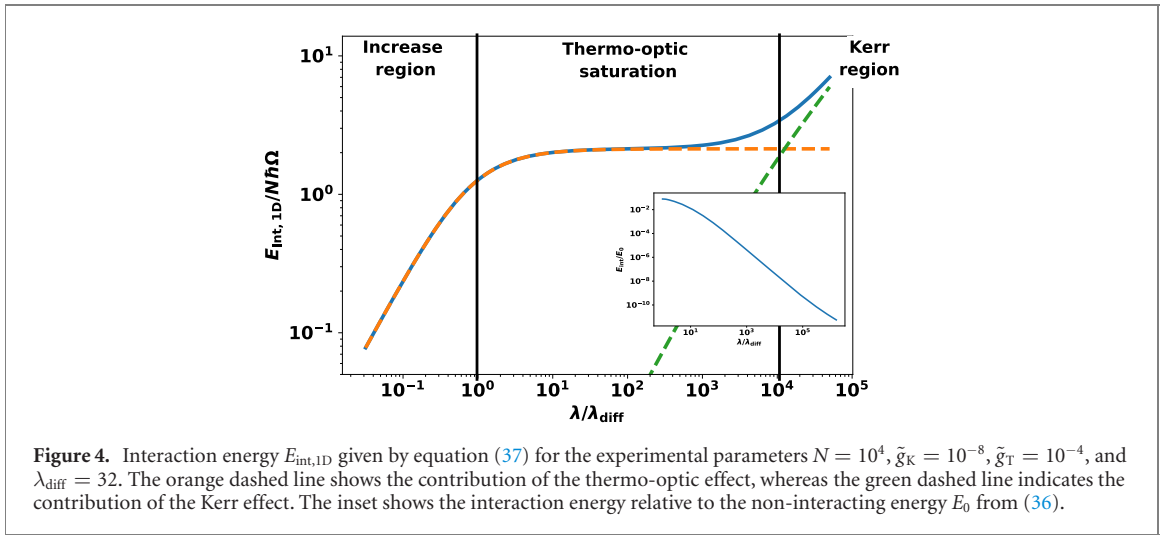
$$\tilde{g}_{1D,\infty}^{exp} = \frac{\lambda_{diff}}{\sqrt{2\pi}} \tilde{g}_T. \tag{34}$$

Therefore, we can, indeed, expect an increase of the effective photon–photon interaction strength via a dimensional crossover. Taking into account that $\lambda_{diff} \sim 32$, the expected increase of the interaction strength amounts to more than one order of magnitude.

3.4. Energy
From analysing the behaviour of the variational parameters, which are basically the widths of the phBEC wave function, at the dimensional crossover it is obvious that the effective photon–photon interaction strength can be measured quite directly. However, we emphasise that this measurement relies on evaluating real space images of the light leaking out the cavity. More precise results are expected from spectroscopic measurements of this light, which directly reveals the phBEC energy. Thus, we discuss now the resulting

Figure 4. Interaction energy $E_{\text{int,1D}}$ given by equation (37) for the experimental parameters $N = 10^4$, $\tilde{g}_{\text{K}} = 10^{-8}$, $\tilde{g}_{\text{T}} = 10^{-4}$, and $\lambda_{\text{diff}} = 32$. The orange dashed line shows the contribution of the thermo-optic effect, whereas the green dashed line indicates the contribution of the Kerr effect. The inset shows the interaction energy relative to the non-interacting energy E_0 from (36).

energy of the condensate in more detail. In the effective 1D case by using $\alpha_y \approx 1$ and the definition (30) of the effective 1D interaction strength from the energy function (21), we find for the energy

$$E_{\text{1D}} \approx \frac{N\hbar\Omega}{2}\left[\frac{1}{2}\left(\frac{1}{\alpha_x^2} + \alpha_x^2\right) + \lambda^2 + \frac{\tilde{g}_{\text{1D}}(\lambda)N}{\sqrt{2\pi}\alpha_x}\right].$$

(35)

This formally coincides with (A.4) from appendix A apart from the λ^2 dependency, which represents the shift of the ground state due to the energy of the squeezed direction. Introducing the non-interacting energy

$$E_0 = \frac{N\hbar\Omega}{2}\left(1 + \lambda^2\right),$$

(36)

we can define the interaction contribution to the energy by

$$E_{\text{int, 1D}} = E_{\text{1D}} - E_0,$$

(37)

which is plotted in figure 4 as a function of the trap aspect ratio λ.

Again, we find the same threefold behaviour we have already observed for the widths and the interaction strength, which stems from a saturation of the thermo-optic interaction for intermediate λ. Moreover, we see from the inset in figure 4 that the interaction energy $E_{\text{int,1D}}$ is quite small compared to the unperturbed energy (36), so that our variational approach is a good approximation of the true ground state.

Finally, we remark that our findings can be measured by utilising the fact that the thermo-optic interaction builds up steadily during the experimental run. At the beginning of the experiment the dye-filled solution in the cavity does not have any temperature difference with respect to the environment, so the thermo-optic interaction does not yet occur, whereas the instantaneous Kerr interaction is already fully present. As a single experiment lasts only about 500 ns, the temperature difference saturates only after several pump pulses, such that then the thermo-optic interaction is in its steady state and yields its full contribution. Consequently, the resulting strength of the thermo-optic interaction can be measured by determining the energy of the condensate at the beginning of the experiment and by comparing it with the energy at the end. In principle this would involve subtracting the Kerr contribution from the interaction energy (37),

$$E_{\text{th, 1D}} = E_{\text{int, 1D}} - \frac{\hbar\Omega\tilde{g}_{\text{K}}\lambda N^2}{2\sqrt{2\pi}\alpha_x}.$$

(38)

However, as already mentioned above, in the experiment only the thermo-optic saturation region is expected to be accessible. According to figure 4 the energy contribution due to the Kerr effect is negligible in the whole experimental regime. According to equation (38) the total interaction energy (37) coincides with the thermo-optic energy contribution. Therefore, one can directly use expression (37) to determine the strength of the effective photon–photon interaction. We remark that for sufficiently small particle number N one can enter the regime where it is valid to determine the variational parameters perturbatively in first order with respect to the smallness parameter $\tilde{g}_{\text{1D}}(\lambda)N/\sqrt{2\pi}$. In this case the interaction energy (37) is directly given by

$$E_{\text{int, 1D}} \approx \frac{\hbar\Omega\tilde{g}_{\text{1D}}(\lambda)N^2}{2\sqrt{2\pi}}.$$

(39)

allowing to directly determine the effective interaction strength from the measured value of $E_{\text{int,1D}}$.

4. Dimensional crossover with constant particle density

So far we have studied the crossover for a constant particle number only. However, increasing the trap aspect ratio implies a corresponding increase of the photon density, so it is unavoidable from an experimental point of view for intrinsic mirror losses to lead the condensate turning multimode [29]. Therefore, we study now a complementary approach to the dimensional crossover, where we fix the geometric mean $\bar{\Omega} = \lambda \Omega_x$, which yields the potential in the form

$$
V = \frac{m\bar{\Omega}^2}{2} \left(\frac{x^2}{\lambda^2} + \lambda^2 y^2 \right). \tag{40}
$$

Thus, increasing the trap-aspect ratio λ tightens the trap in the y-direction while loosening the trapping potential in the x-direction. Due to this, the photon density in the trap centre stays the same throughout the whole crossover. However, note that the exact 1D limit, i.e. $\lambda \to \infty$ corresponds to a free particle in x-direction. In this situation a suitable ansatz function for a minimisation procedure is given by

$$
\psi = \sqrt{\frac{N}{\bar{\alpha}_x \bar{\alpha}_y \pi \bar{l}^2}} \, \exp\left[-\frac{1}{2\bar{l}} \left(\frac{x^2}{\lambda \bar{\alpha}_x^2} + \frac{\lambda y^2}{\bar{\alpha}_y^2} \right) \right], \tag{41}
$$

where $\bar{l} = l_x/\sqrt{\lambda}$ denotes the geometric mean of the oscillator lengths and $\bar{\alpha}_x, \bar{\alpha}_y$ are the new variational constants. Inserting ansatz (41) into the energy functional (15) with the potential (40) yields for the energy the expression

$$
\bar{E} = \frac{N\hbar\bar{\Omega}}{4} \left(\frac{1}{\lambda \bar{\alpha}_x^2} + \frac{\bar{\alpha}_x^2}{\lambda} + \frac{\lambda}{\bar{\alpha}_y^2} + \lambda \bar{\alpha}_y^2 + \frac{\tilde{g}_K N}{\pi \bar{\alpha}_x \bar{\alpha}_y} + \frac{\tilde{g}_T N}{\pi \bar{\alpha}_x \bar{\alpha}_y} I \right), \tag{42}
$$

where I abbreviates the integral

$$
I = \int_0^\infty \mathrm{d}t \, \frac{e^{-t}}{\sqrt{\left[1 + 2t/(\bar{\alpha}_y^2 \lambda_{\text{diff}}^2) \right] \left[1 + 2t/(\bar{\alpha}_x^2 \lambda_{\text{diff}}^2 \lambda^2) \right]}}. \tag{43}
$$

Here we can approximate $I \approx 1$ since both factors in the root can be treated as explained below equation (24). This implies, that in this situation the Kerr interaction and the thermo-optic interaction behave identically and only the total interaction strength $\tilde{g} = \tilde{g}_K + \tilde{g}_T$ appears. On the other hand this also implies, that a saturation effect of the thermo-optic interaction, as found in the proceeding section, does not exist here and, therefore, a larger effective photon–photon interaction is achievable. We derive from the energy (42) the following equations for the variational parameters

$$
\bar{\alpha}_x = \frac{1}{\bar{\alpha}_x^3} + \frac{\tilde{g}\lambda N}{2\pi \bar{\alpha}_x^2 \bar{\alpha}_y}, \tag{44}
$$

in the x-direction and for the y-direction we have

$$
\bar{\alpha}_y = \frac{1}{\bar{\alpha}_y^3} + \frac{\tilde{g}N}{2\pi \lambda \bar{\alpha}_x \bar{\alpha}_y^2}. \tag{45}
$$

Figure 5(a) shows a numerical solution of the coupled equations (44) and (45) for the experimentally relevant parameters $N = 10^4$, $\tilde{g}_K = 10^{-8}$ and $\tilde{g}_T = 10^{-4}$. We see also here, that for increasing trap-aspect ratio the variational parameter $\bar{\alpha}_y$ in the squeezed direction attends the value 1, implying the interaction in this direction to be less relevant. Secondly, we note the monotonous increase of the variational parameter in the x direction in contrast to the previous results indicating the absence of a saturation effect. Therefore, larger condensate widths and, thus, larger effective photon–photon interactions are reachable. Moreover, also here we perform a numerical evaluation of the original equations (1) and (2) as above, which perfectly agrees with the evaluation of the variational equations (44) and (45).

For increasing trap-aspect ratio λ we note in (45) that the interaction term vanishes. Taking approximately $\bar{\alpha}_x \approx 1$ and $\bar{\alpha}_y \approx 1$ again reveals the 1D criterion (27). For evaluating the effective 1D behaviour we stay as above with the approximation $\bar{\alpha}_y \approx 1$ and insert this into equation (44). We end up with

$$
\bar{\alpha}_x^4 \approx 1 + \frac{\tilde{g}\lambda N}{2\pi} \bar{\alpha}_x. \tag{46}
$$
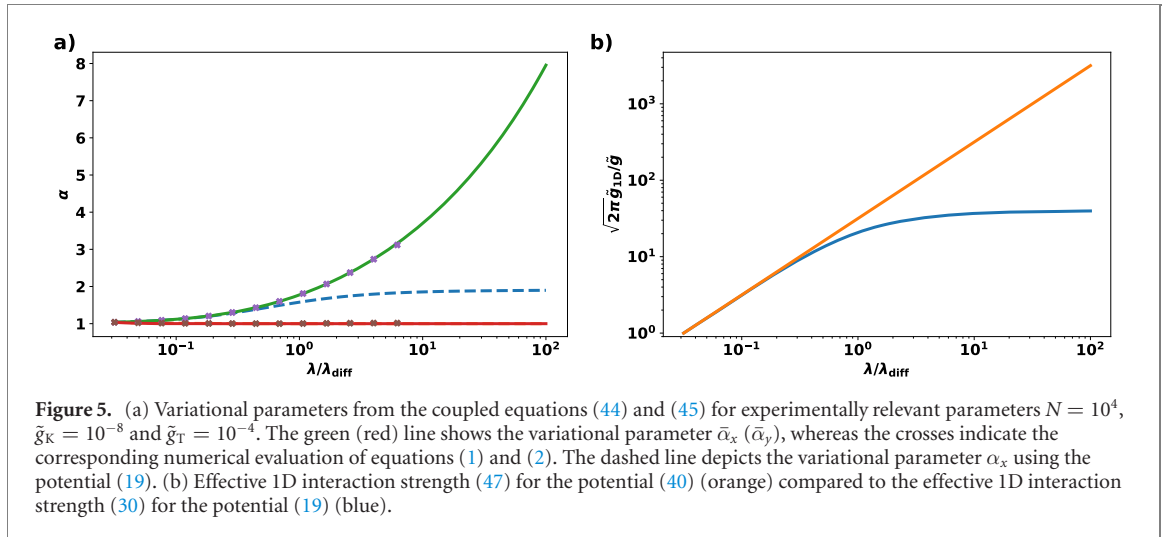
Figure 5. (a) Variational parameters from the coupled equations (44) and (45) for experimentally relevant parameters $N = 10^4$, $\tilde{g}_K = 10^{-8}$ and $\tilde{g}_T = 10^{-4}$. The green (red) line shows the variational parameter $\bar{\alpha}_x$ ($\bar{\alpha}_y$), whereas the crosses indicate the corresponding numerical evaluation of equations (1) and (2). The dashed line depicts the variational parameter α_x using the potential (19). (b) Effective 1D interaction strength (47) for the potential (40) (orange) compared to the effective 1D interaction strength (30) for the potential (19) (blue).

Thus, comparing (A.6) with (46) yields for the effective 1D interaction strength in the current crossover setting governed by the potential (40) a linear increase with the trap-aspect ratio

$$\bar{\bar{g}}_{1D}(\lambda) = \frac{\tilde{g}\lambda}{\sqrt{2\pi}}. \tag{47}$$

As already mentioned in the beginning of this section, indeed, no saturation regime for the thermo-optic interaction is observed in this setting and, consequently, even larger effective interaction constants can be achieved. A comparison of the interaction strength (47) with the previously derived interaction strength (30) is shown in figure 5(b). Whereas the interaction strength (30) saturates for larger anisotropies the new interaction strength (47) grows linearly for all values of the trap-aspect ratio.

5. Summary

In this paper we have shown how the ground state of a phBEC changes during the dimensional crossover from 2D to 1D. Our main focus in this investigation was the behaviour the effective photon–photon interaction strength in the crossover in order to make effects like superfluidity accessible in experiments. We have found that the effective photon–photon interaction strength increases through the crossover. However, we have shown that the thermo-optic interaction can only be increased up to a factor $\lambda_{diff}/\sqrt{2\pi}$, cf section 3.3. The deeper physical reason behind this finding is that for large enough trap aspect ratio a large amount of energy is carried away by the heat diffusion from the region occupied by the condensate and cannot contribute to the interaction anymore. Contrarily to that, the Kerr interaction increases linearly with the trap aspect ratio such that for a large trap anisotropy, which is presumably not achievable in current experiments, the Kerr interaction gives the leading interaction effect. Therefore, we have shown that the effective photon–photon interaction may be increased by more than an order of magnitude compared to the currently available experiments in 2D. We also work out a complementary dimensional crossover scenario, where an additional loosing of the confinement of the second dimension results in a linear growth of the effective 1D interaction constant by more than an order of magnitude. In conclusion, we show that the behaviour of the condensate in the effective 1D limit depends on the details of how the dimensional crossover is performed concretely.

Acknowledgments

Data availability statement

All data that support the findings of this study are included within the article (and any supplementary files).

Appendix A. 1D Gross–Pitaevskii equation

In order to compare the results from the dimensional crossover to the exact 1D scenario, we review in this section the steady state of a one-dimensional Gross–Pitaevskii equation with harmonic trapping potential. Thus, we have to solve

$$\mu\psi = \left(-\frac{\hbar^2\nabla^2}{2m} + \frac{m\Omega^2}{2}x^2 + g_{1D}|\psi|^2 \right)\psi, \tag{A.1}$$

with the corresponding functional

$$E_{1D}[\psi,\psi^*] = \frac{\hbar^2}{2m}\int dx\, |\partial_x\psi|^2 + \frac{m\Omega^2}{2}\int dx\, x^2|\psi|^2 + \frac{g_{1D}}{2}\int dx|\psi|^4. \tag{A.2}$$

In order to obtain an approximate solution, we use a Gaussian ansatz function

$$\psi = \sqrt{\frac{N}{\sqrt{\pi}l\alpha}}e^{-x^2/(2l^2\alpha^2)}, \tag{A.3}$$

where $l = \sqrt{\hbar/(m\Omega)}$ stands for the oscillator length and α represents the dimensionless variational parameter. Inserting ansatz (A.3) in the energy functional (A.2) yields for the energy

$$E_{1D} = \frac{\hbar\Omega}{2}\left(\frac{1}{2\alpha^2} + \frac{\alpha^2}{2} + \frac{\tilde{g}_{1D}N}{\sqrt{2\pi}\alpha} \right), \tag{A.4}$$

where we define the dimensionless 1D interaction strength [30, section 15.3.2]

$$\tilde{g}_{1D} = \frac{g_{1D}ml}{\hbar^2}. \tag{A.5}$$

Extremising (A.4) with respect to the dimensionless width α, we obtain the algebraic equation

$$\alpha^4 = 1 + \frac{N\tilde{g}_{1D}}{\sqrt{2\pi}}\alpha. \tag{A.6}$$

ORCID iDs

Enrico Stein https://orcid.org/0000-0003-4820-7126
Axel Pelster https://orcid.org/0000-0002-5215-0348

References

[1] Bloch I, Dalibard J and Zwerger W 2008 Many-body physics with ultracold gases *Rev. Mod. Phys.* **80** 885
[2] Giamarchi T 2003 *Quantum Physics in One Dimension* (Oxford: Oxford University Press)
[3] Hadzibabic Z, Krüger P, Cheneau M, Battelier B and Dalibard J 2006 Berezinskii–Kosterlitz–Thouless crossover in a trapped atomic gas *Nature* **441** 1118
[4] Fletcher R J, Robert-de-Saint-Vincent M, Man J, Navon N, Smith R P, Viebahn K G H and Hadzibabic Z 2015 Connecting Berezinskii–Kosterlitz–Thouless and BEC phase transitions by tuning interactions in a trapped gas *Phys. Rev. Lett.* **114** 255302
[5] Christodoulou P, Gałka M, Dogra N, Lopes R, Schmitt J and Hadzibabic Z 2021 Observation of first and second sound in a BKT superfluid *Nature* **594** 191
[6] Dettmer S *et al* 2001 Observation of phase fluctuations in elongated Bose–Einstein condensates *Phys. Rev. Lett.* **87** 160406
[7] Cazalilla M A, Ho A F and Giamarchi T 2006 Interacting Bose gases in quasi-one-dimensional optical lattices *New J. Phys.* **8** 158
[8] Delfino F and Vicari E 2017 Dimensional crossover of Bose–Einstein-condensation phenomena in quantum gases confined within slab geometries *Phys. Rev. A* **96** 043623
[9] Vogler A, Labouvie R, Barontini G, Eggert S, Guarrera V and Ott H 2014 Dimensional phase transition from an array of 1D Luttinger liquids to a 3D Bose–Einstein condensate *Phys. Rev. Lett.* **113** 215301
[10] Irsigler B and Pelster A 2017 Dimensionally induced one-dimensional to three-dimensional phase transition of the weakly interacting ultracold Bose gas *Phys. Rev. A* **95** 043610
[11] Görlitz A *et al* 2001 Realization of Bose–Einstein condensates in lower dimensions *Phys. Rev. Lett.* **87** 130402
[12] Klaers J, Schmitt J, Vewinger F and Weitz M 2010 Bose–Einstein condensation of photons in an optical microcavity *Nature* **468** 545
[13] Maruo S, Nakamura O and Kawata S 1997 Three-dimensional microfabrication with two-photon-absorbed photopolymerization *Opt. Lett.* **22** 132

[14] Deubel M, von Freymann G, Wegener M, Pereira S, Busch K and Soukoulis C M 2004 Direct laser writing of three-dimensional photonic-crystal templates for telecommunications *Nat. Mater.* **3** 444

[15] Hohmann J K, Renner M, Waller E H and von Freymann G 2015 Three-dimensional μ-printing: an enabling technology *Adv. Opt. Mater.* **3** 1488

[16] Stein E and Pelster A 2021 Thermodynamics of trapped photon gases at dimensional crossover from 2D to 1D (arXiv:2011.06339)

[17] Bagnato V and Kleppner D 1991 Bose–Einstein condensation in low-dimensional traps *Phys. Rev.* A **44** 7439

[18] Ketterle W and van Druten N J 1996 Bose–Einstein condensation of a finite number of particles trapped in one or three dimensions *Phys. Rev.* A **54** 656

[19] Yukalov V I 2005 Modified semiclassical approximation for trapped Bose gases *Phys. Rev.* A **72** 033608

[20] Petrov D S, Shlyapnikov G V and Walraven J T M 2000 Regimes of quantum degeneracy in trapped 1D gases *Phys. Rev. Lett.* **85** 3745

[21] Klaers J, Vewinger F and Weitz M 2010 Thermalization of a two-dimensional photonic gas in a 'white wall' photon box *Nat. Phys.* **6** 512

[22] Stein E, Vewinger F and Pelster A 2019 Collective modes of a photon Bose–Einstein condensate with thermo-optic interaction *New J. Phys.* **21** 103044

[23] Klaers J, Schmitt J, Damm T, Vewinger F and Weitz M 2011 Bose–Einstein condensation of paraxial light *Appl. Phys.* B **105** 17

[24] Damm T, Schmitt J, Liang Q, Dung D, Vewinger F, Weitz M and Klaers J 2016 Calorimetry of a Bose–Einstein-condensed photon gas *Nat. Commun.* **7** 11340

[25] Salasnich L, Parola A and Reatto L 2002 Effective wave equations for the dynamics of cigar-shaped and disk-shaped Bose condensates *Phys. Rev.* A **65** 043614

[26] Kleinert H and Schulte-Frohlinde V 2001 *Critical Properties of Φ^4 Theories* (Singapore: World Scientific)

[27] Gradshteyn I S and Ryzhik I M 2007 *Table of Integrals, Series, and Products* 7th edn (Amsterdam: Elsevier)

[28] Vewinger F and von Freymann G 2021 Private communication

[29] Hesten H J, Nyman R A and Mintert F 2018 Decondensation in nonequilibrium photonic condensates: when less is more *Phys. Rev. Lett.* **120** 040601

[30] Pethick C J and Smith H 2008 *Bose–Einstein Condensation in Dilute Gases* 2nd edn (Cambridge: Cambridge University Press)